Optik 124 (2013) 570–574

Contents lists available at SciVerse ScienceDirect

Optik

journal homepage: www.elsevier.de/ijleo

Structural and optoelectronic properties of NiTiX and CoVX (X = Sb and Sn) half-Heusler compounds: An ab initio study

M. Ameri[a], A. Touia[a], R. Khenata[b], Y. Al-Douri[c,*], H. Baltache[b]

[a] Département de Physique, Faculté des Sciences, Université Djillali LIABES, Sidi-Bel-Abbès, 22000, Algeria
[b] Laboratoire de Physique Quantique et de Modélisation Mathématique de la Matière, (LPQ3M), Centre universitaire de Mascara, Mascara, 29000, Algeria
[c] Institute of Nono Electronic Engineering, University Malaysia Perlis, 01000 Kangar, Perlis, Malaysia

ARTICLE INFO

Article history:
Received 4 August 2011
Accepted 17 December 2011

PACS:
61.50.Ks
62.30.+d
71.18.+y
71.20.Nr

Keywords:
Half-Heusler alloys
Structural properties
Effective mass
FP-LMTO

ABSTRACT

We have performed ab-initio self-consistent calculations using the full-potential linear muffin-tin orbital (FP-LMTO) method to investigate the structural and the electronic properties of some half-Heusler alloys. The local density and generalized gradient approximations were used for NiTiSn and CoVSn alloys. Due to the metallic characters of both NiTiSb and CoVSb compounds, the local spin density approximation was used. Lattice constants, bulk moduli, and the pressure derivatives of the bulk moduli are calculated, band structure and density of states are drawn and effective masses are investigated. To our knowledge this is the first quantitative theoretical prediction of the effective masses for the investigated compounds and still awaits experimental confirmations. The obtained results are agreed well with the other published values.

1. Introduction

The family of half-Heusler phases includes well over 100 phases and have been studied extensively in recent years [1–9]. Half-Heusler phases are known to form from a wide variety of different elements and in a typical phase with general formula XYZ, X is a heavy transition metal, Y is a light transition metal or a rare-earth metal, and Z is a late main-group element (most frequently Sb or Sn). These phases exhibit a great variety of electronic states and physical properties. The properties of the half-Heusler phases vary somewhat systematically with the valence-electron content (VEC; note, valences prescribed by the periodic table) as manifested, e.g., by changes in electronic conductivity and magnetic characteristics with VEC [3–10]. Semiconducting features are associated with VEC = 8 and 18, which represent highly preferred electron configurations fulfilling the octet or expanded octet rule. So-called half-metallic ferromagnetic (HMF) materials are found among phases with VEC = 22 [11–13]. These phases have large magnetic moments and in the electronic structure of these phases the majority-spin channel exhibits metallic characteristics, while the minority-spin channel exposes a semiconductor-like gap at the Fermi level (F).

As the considered compounds corresponds to the variation of the valence electron number from 18 (NiTiSn and CoVSn), to 19 (NiTiSb and CoVSb). Considering the physical properties, compounds such as NiTiSn and CoVSn with EC = 18 were found to be semiconductors (SC), in contrast with those of EC = 19 such as NiTiSb and CoVSb are considered as weak ferromagnet. To understand some of the physical properties of these compounds, a detailed description of the electronic structure is needed. The aim of this work is to provide a comparative study of structural–electronic properties using the full-potential muffin-tin orbital (FP-LMTO) method. Quantities including lattice parameters, bulk modulus and electronic structure were obtained for these compounds.

2. Computational method

The half-Heusler XYZ compounds crystallize in the face centered cubic structure with one formula unit per unit cell. The space group is *F*4/3*m* (No. 216). Y and Z atoms are located at 4a (0,0,0) and 4b (1/2,1/2,1/2) position forming the rock salt structure arrangement. The X atom is located in the octahedral coordinated pocket at one of the cube center positions 4c (1/4,1/4,1/4) leaving the

* Corresponding author. Tel.: +60 4 9775021; fax: +60 4 9798578.
E-mail address: yaldouri@yahoo.com (Y. Al-Douri).

0030-4026/$ – see front matter © 2012 Elsevier GmbH. All rights reserved.
doi:10.1016/j.ijleo.2011.12.052

Table 1
The number of plane wave (NPW), energy cut-off (in Ry) and the muffin-tin radius (MTS) (in a.u.), used in our calculations.

	NiTiSn			NiTiSb			CoVSn			CoVSb		
NLW												
LDA	5064			–			5064			–		
GGA	9984			–			9984			–		
LSDA	–			5064			–			5064		
Ecut-off (Ry)												
LDA	93.47			–			97.7			–		
GGA	139.66			–			146.53			–		
LSDA	–			93.42			–			97		
MTS (a.u.)	Ni	Ti	Sn	Ni	Ti	Sb	Co	V	Sn	Co	V	Sb
LDA	2.24	2.53	2.53	–	–	–	2.19	2.47	2.47	–	–	–
GGA	2.29	2.59	2.59	–	–	–	2.29	2.48	2.48	–	–	–
LSDA	–	–	–	2.24	2.53	2.53	–	–	–	2.20	2.48	2.48

other 4d (3/4,3/4,3/4) empty. When the Z atomic positions are empty the structure is analogous to zinc blend structure which is common for large number of semiconductors. The calculations reported here were performed using the FP-LMTO method within the density-functional theory (DFT) [14,15]. The local density and generalized gradient approximations (LDA and GGA) have been used for the exchange-correlation (XC) for the semiconductor compounds [16,17]. The local spin density approximation (LSDA) [16] is used for the metallic compounds. The present method is an improved one compared to previous LMTO methods. The FP-LMTO method treats muffin-tin spheres and interstitial regions on the same footing, leading to improvements in the precision of the eingenvalues. At the same time, the FP-LMTO method, in which the space is divided into an interstitial regions (IR) and non overlapping muffin-tin spheres (MTS) surrounding the atomic sites, uses a more complete basis than its predecessors. In the IR regions, the basis functions are represented by Fourier series. Inside the MTS, the basis functions are represented in terms of numerical solutions of the radial Schrödinger equation for the spherical part of the potential multiplied by spherical harmonics. The charge density and the potential are represented inside the MTS by spherical harmonics up to $l_{max} = 6$. The k-points integration over the Brillouin zone is performed using the tetrahedron method [18]. The values of the sphere radii used in our calculation are listed in Table 1.

3. Results and discussion

3.1. Structural properties

The total energy–volume variation for NiTiSn and CoVSn compounds were calculated using both LDA and GGA approximations for the exchange-correlation potential. Whereas, for the metallic compounds NiTiSb and CoVSb the LSDA was used. The energy–volume variation of two families was fitted to the Birch's equation of state [19]. The fitted results including the equilibrium lattice constants, bulk moduli and their pressure derivatives are listed in Table 2. The equilibrium lattice constant is compared with other theoretical results. It is observed that our calculated lattice constants using LDA are smaller than the theoretical values, while our GGA results are larger. The bulk modulus should be quite good indicator of hardness, since it is related to an isotropic deformation. From the calculated bulk moduli listed in Table 2, it is seen that CoVSb is more hardness than other half Heusler compounds. Since we have not neither theoretical nor experimental values to compare with, we leave these investigated results as a reference for future verification.

3.2. Electronic structure

3.2.1. CoVSb and NiTiSb

The calculated spin-polarized band structures for CoVSb and NiTiSb compounds at the predicted equilibrium lattice constants are depicted in Fig. 1, which is drawn along the symmetry in the first Brillouin zone. We defined the majority spin component to be the one contains the largest number of electrons. For CoVSb (Fig. 1a), the majority spin band is metallic, while the minority spin is semiconductor, the band gap is much wider than 1.8 eV, and the top of the valence band is reduced to under the Fermi level (E_F). The states in the energy range −12.5 to −10 eV, are mainly from 5s-Sb states, the region between −6 eV and −3.5 eV is due to Co-4s and V-4s with small contributions from 5p-Sb, 4p-Co and 4p-V, the remaining part from −3.5 eV up to Fermi energy is essentially dominated by 3d-V and 3d-Co states with the minor contributions from 5d-Sb states. The group from E_F up to 1.59 eV is dominated by Co-3d and V-3d states. Then after, there are preponderance of 4s/5s-V, and 5p-Sb states.

In case of NiTiSb compound, the majority and minority spin band show similar features as depicted in Fig. 1b. The lowest group situated between −12.68 eV and −10.65 eV (not shown) is dominated by 5s-Sb with contribution from 4s-Ni. The group between (−6.21 and −3.84 eV) is dominated by 5p-Sb with minor contributions from 4s-Ni and 4s-Ti. The region below E_F is mainly from 3d-Ni. The group around E_F is dominated by 3d-Ti. The contribution of Ni-3d and Ti-3d states for the majority spin systems can be divided in two parts. First, the band originating from the Ni-3d ($x^2 - y^2$ and $3z^2 - 1$) (e_g doubly degenerate state) orbitals is located at −3.9 to −1.8 eV. Second, the Mn-3d (yz, zx and xy) triply degenerate band is centered at −3.9 eV. In contrast, the Ti-3d is a triplet, centered between −1 and 1 eV and a doublet in the region including the Fermi energy.

To further elucidate the nature of the electronic band structure, we have also calculated the total density of state (DOS) as displayed in Fig. 2, where distinguished three structures below E_F, the first one arises entirely from 5p-Sb with minor contributions from 4s-V and 4s-Co states. The remaining structures are entirely dominated by 3d-V and 3d-Co states. The hybridization effect is stronger for the 3d-Co states (the Co d states are split into a doublet with e_g symmetry and triplet with t_{2g} symmetry, respectively). The region just beyond E_F is essentially dominated by d states of these elements.

Fig. 2 shows the similarity between the majority and minority spin, the lowest part below E_F is mainly due to the 5s-Sb states with a small contribution of 4s-Ni. The remaining part is essentially dominated by Ni-3d states with the contributions from Ti-3d states. The structure around E_F is dominated by Ti-3d states, the structure from 1.5 eV and above are consist of mixture of the Ni-4s,4p, Ti-4s,4p and Sb-5s,5p states.

Table 2
Calculated lattice parameter a, bulk modulus B and its pressure derivatives B' for NiTiX and CoVX (X = Sb,Sn) compounds, compared to other theoretical values.

	a_0 (Å)	B (GPa)	B'
NiTiSn			
Present work	5.835^{LDA}, 5.973^{GGA}	147.81^{LDA}, 124.58^{GGA}	4.18^{LDA}, 4.015^{GGA}
Others	5.941[a,b], 5.947[c]		
NiTiSb			
Present work	5.84	142.67	4.89
Others	5.872[a,b]		
CoVSn			
Present work	5.706^{LDA}, 5.831^{GGA}	167.96^{LDA}, 154.14^{GGA}	4.39^{LDA}, 3.68^{GGA}
Others	5.98[b]		
CoVSb			
Present work	5.73	173.554	3.632
Others	5.80[a], 5.766[b], 5.791[c]		

[a] Ref. [3], Theo.
[b] Ref. [20], Theo.
[c] Ref. [2] Theo.

3.2.2. CoVSn and NiTiSn

The calculated electronic band structures of both NiTiSn and CoVSn compounds are shown in Fig. 3. Following this figure, the valence band maximum (VBM) is located at Γ and L points for NiTiSn and CoVSn, respectively. The conduction band minimum (CBM) is located at X point for both compounds, resulting in an indirect energy band gap (Γ–X) for NiTiSn and (L–X) for CoVSn. The calculated band gap value is found to be 0.47 eV within LDA and 0.436 eV within GGA for NiTiSn compound. For CoVSn compound the energy gap is about 0.66 and 0.64 eV for LDA and GGA respectively. Our calculated energy band gap is in good agreement with the value obtained by Tobola and Pierre [3]. Comparing the band structures around the Γ point below the Fermi level, we see that three bands are degenerate in this region. From the total DOS (Fig. 4), it is seen that just below E_F, the bands are dominated by 3d-X and Y element, with some contribution coming from 5p-Sn states. In the region above the E_F, 3d states of the Y element also dominate with minor contribution of 3d-X element. The states in the energy range −4.5 to −3.5 mainly from 4s states of the X and Y element.

On the other hand, it is also interesting to discuss the effective masses of electrons and holes, which are important for the excitonic properties that are particularly of great interest for such compounds. We have investigated the effective mass of electrons and holes using both LDA and GGA schemes. A theoretical effective mass, in general, turns out to be a tensor with nine components. However, for the very idealized simple case where $E(k)$ is a parabola at $k = 0$ the effective masse becomes a scalar. We have computed the effective masses of electrons and holes at CBM and VBM. The effective masses are obtained by calculating the energies along Δ and Λ directions for Γ point and along Δ and W directions for X point. We have used 1% along the X and L points for Γ and along Δ and W

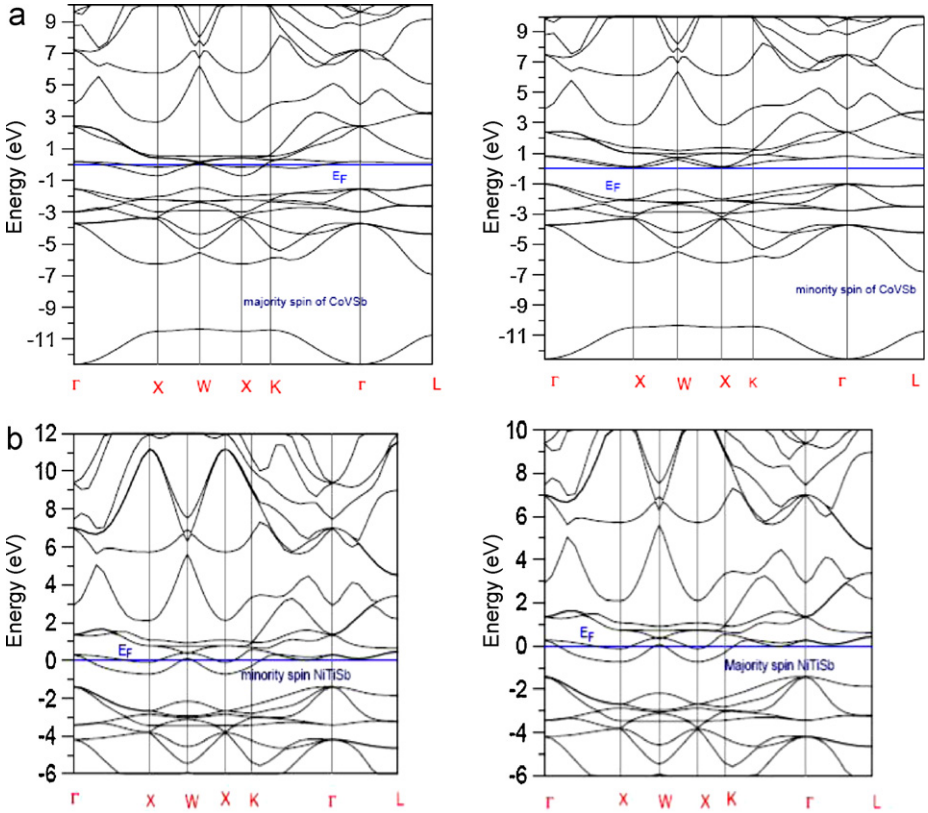

Fig. 1. Spin-polarized band structures of CoVSb (a) and (b) NiTiSb.

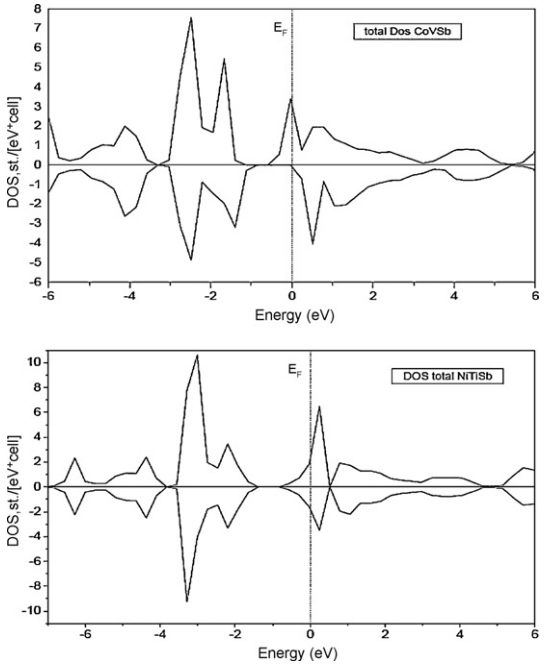

Fig. 2. Total density of state (TDOS) of CoVSb and NiTiSb. The vertical line corresponds to the Fermi energy.

for X. The same results are found along both directions in both Γ and X points fitting on the well-known equation $E = p^2k^2/2m^*$. Our results concerning the light and heavy holes are 0.165 and 0.472 by using LDA (0.175, 0.492 by GGA) for NiTiSn and 0.298, 0.574 by LDA (0.331, 0.672 by GGA) for CoVSn. While for the case of electron masses, our results are 0.222 and 0.245 for NiTiSn (0.626 and 0.692 for CoVSn) using LDA and GGA respectively. It is clearly seen that the GGA values are higher than the LDA values. We note that the

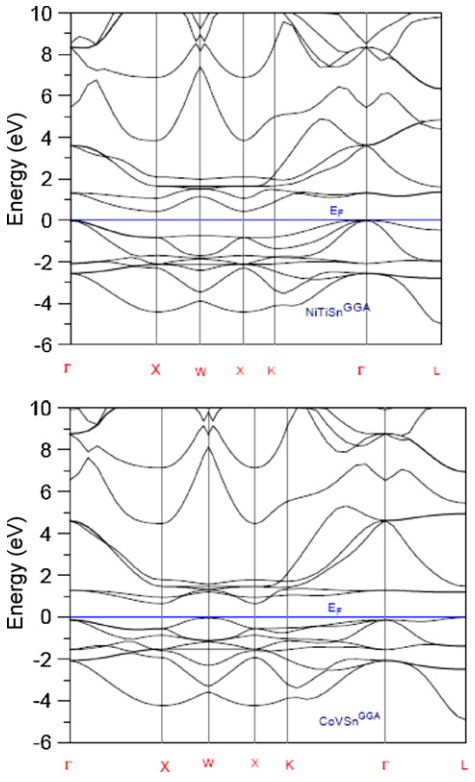

Fig. 3. Band structures of NiTiSn and CoVSn.

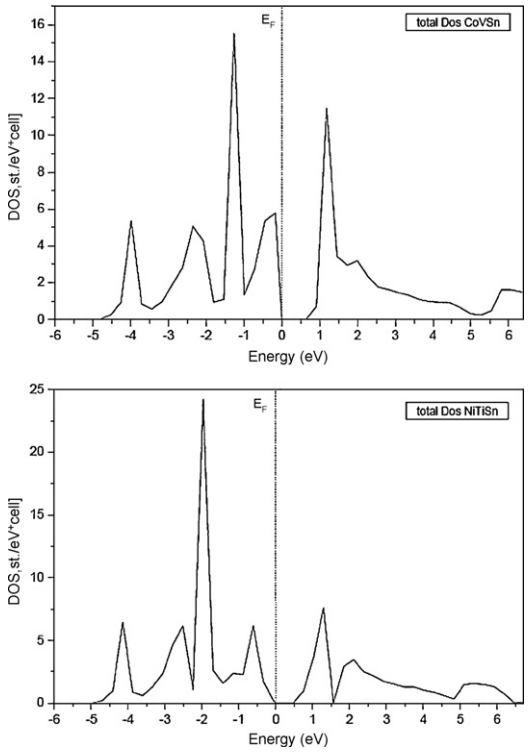

Fig. 4. Total density of state (TDOS) of CoVSn and NiTiSn. The vertical line corresponds to the Fermi energy.

results of CoVSn are higher than NiTiSn. This is consistent with the fact that the VBM along point Γ for CoVSn is reduced under Fermi level.

4. Conclusions

We have performed detailed investigation on the structural and electronic properties of the half-Heusler compounds using first principle FP-LMTO method within LDA, GGA and LSDA schemes. The most relevant conclusions are summarized as follows: (i) the calculated ground state properties such as lattice parameter are in fairly good agreement with the available theoretical values. (ii) We do not aware any theoretical and experimental results of the bulks modulus values. Our results show that the CoVSb compound exhibits more hardness than other compounds. (iii) Our results for the band structure show, that NiTiSn and CoVSn are semiconductors, whereas, NiTiSb and CoVSb are metallic. (vi) The calculated effective masses of the compounds are investigated. (vii) To the best of our knowledge, there are no earlier studies of the effective masses of electrons and holes of these compounds; we feel that our calculations can be used to cover the lack of data for these compounds.

Acknowledgments

One of us, (Y.A.) would like to acknowledge the finanicial support presented by FRGS grants numbered: 9003-00249 & 9003-00249 and TWAS-Italy for the full support of his visit to JUST-Jordan under TWAS-UNESCO Associateship. Also, (R. Kh.) extends his appreciation to the Deanship of Scientific Research at King Saud University for funding

the work through the research group project no. RGP-VPP-088.

References

[1] I. Galanakis, P.H. Dederichs, Half-Metallic alloys Fundamentals and Applications, Springer, Berlin Heidelberg, 2005.
[2] J. Pierre, R.V. Skolozdra, J. Tobola, S. Kaprzyk, C. Hordequin, M.A. Koua-cou, I. Karla, R. Currat, E. Lelièvre-Berna, Properties on request in semi-Heusler phases, J. Alloys Compd. 262/263 (1997) 101–107.
[3] J. Tobola, J. Pierre, Electronic phase diagram of the XTZ (X = Fe, Co, Ni; T = Ti, V, Zr, Nb, Mn; Z = Sn, Sb) semi-Heusler compounds, J. Alloys Compd. 296 (2000) 243–252.
[4] I. Galanakis, Orbital magnetism in the half-metallic Heusler alloys, Phys. Rev. B 71 (2005) 12413–12416.
[5] L. Offernes, P. Ravindran, C.W. Seim, A. Kjekshus, Prediction of composition for stable Half-Heusler phase from electronic band structure analysis, J. Alloys Compd. 458 (2008) 47–60.
[6] T. Block, M.J. Carey, B.A. Gurney, O. Jepsen, Band-structure calculations of the half-matallic ferromagnetism and structural stability of full- and half-Heusler phases, Phys. Rev. B 70 (2004) 205114–205118.
[7] F.B. Mancoff, J.F. Bobo, O.E. Richter, K. Bessho, P.R. Johnson, R. Sinclair, W.D. Nix, R.L. White, B.M. Clemens, Growth and characterization of epitaxial NiMnSb/PtMnSb C1b Heusler alloy superlattices, J. Mater. Res. 14 (1999) 1560–1569.
[8] R.A. de Groot, F.M. Mueller, P.G. Van Engen, K.H.J. Buschow, Half-metallic ferromagnets and their magneto-optical properties, J. Appl. Phys. 55 (1984) 2151–2154.
[9] Y. Xia, S. Bhattacharya, V. Ponnambalam, A.L. Pope, S.J. Poon, T.M. Tritt, Thermoelectric properties of semimetallic (Zr,Hf) CoSb half-Heusler phases, J. Appl. Phys. 88 (2000) 1952–1955.
[10] J. Tobola, J. Pierre, S. Kaprzyk, R.V. Skolozdra, M.A. Kouacou, Electronic and structural properties of two semi-Heusler alloys: NbIrSn and NbIrSb, J. Phys.: Condens. Matter 10 (1998) 1013–1032.
[11] R.A. de Groot, K.H.J. Buschow, Recent developments in half-metallic magnetism, J. Magn. Magn. Mater. 54–57 (1986) 1377–1380.
[12] E.T. Kulatov, Y.A. Uspenskii, S.V. Halilov, Ab initio calculated magneto-optical spectra of half metallic ferromagnets with $C1_b$ structure, Phys. Lett. A 195 (1994) 267–270.
[13] P.A. Dowben, R. Skomski, Are half-metallic ferromagnets half metals? J. Appl. Phys. 95 (2004) 7453–7458.
[14] S. Savrasov, D. Savrasov, Full-potential linear-muffin-tin-orbital method for calculating total energies and forces, Phys. Rev. B 46 (1992) 12181–12195.
[15] S.Y. Savrasov, Linear-response theory and lattice dynamics: a muffin-tin-orbital approach, Phys. Rev. B 54 (1996) 16470–16486.
[16] J.P. Perdew, Y. Wang, Phys. Rev. B 46 (1992) 12947–12954.
[17] J.P. Perdew, K. Burke, M. Ernzerhof, Generalized gradient approximation made simple, Phys. Rev. Lett. 77 (1996) 3865–3868.
[18] P. Blochl, O. Jepsen, O.K. Andersen, Improved tetrahedron method for Brillouin-zone integrations, Phys. Rev. B 49 (1994) 16223–16233.
[19] F. Birch, Finite strain isotherm and velocities for single-crystal and polycrystalline NaCl at high pressures and 300 K, J. Geophys. Res. 83 (1978) 1257–1268.
[20] L. Offernes, P. Ravindran, A. Kjekshus, Electronic structure and chemical bonding in half-Heusler phases, J. Alloys Compd. 439 (2007) 37–54.